A Basic Domain-Derived Tripeptide Inhibits MITF Activity by Reducing its Binding to the Promoter of Target Genes

Dongyoung Lim[1,7], Kyoung-Jin Lee[1,7], Yuri Kim[1], Minseo Kim[1], Hyun-Mi Ju[1], Myoung-Ju Kim[1], Dong-Hwa Choi[2], Jiwon Choi[3], Suree Kim[4,5], Dongmin Kang[4], Kyoungyul Lee[6] and Jang-Hee Hahn[1]

The keratinocytes in UV-irradiated skin produce and secrete α-melanocyte-stimulating hormone. α-Melanocyte-stimulating hormone upregulates the expression of MITF in melanocytes through the cAMP–protein kinase A–CREB signaling pathway. Thereafter, MITF induces the expression of melanogenic genes, including the tyrosinase gene *TYR* and *TYRP-1* and *TYRP-2* genes, which leads to the synthesis and accumulation of melanin. In this study, we examined whether MITF basic region-derived tripeptides can bind to the DNA-binding domain of MITF and inhibit MITF-induced melanogenesis through the inhibition of MITF–DNA binding. MITF-KGR, a representative MITF-derived tripeptide, suppressed the transcriptional activity of MITF by disrupting its binding to the promoter region of the target genes, which resulted in the inhibition of skin epidermis thickness and melanin synthesis in vivo and in vitro. Our results indicate that MITF-KGR exerts an inhibitory effect on melanogenesis by targeting MITF.

Journal of Investigative Dermatology (2021) ■, ■–■; doi:10.1016/j.jid.2021.01.037

INTRODUCTION

Melanogenesis is a multistep biosynthesis process of melanin. Melanin is synthesized in the melanosome of melanocytes (Maresca et al., 2015). Various intrinsic and extrinsic factors affect the synthesis of melanin, such as hormonal proteins, aging, and long-term UV light exposure (D'Mello et al., 2016). The long-term exposure to UVR, especially UVB (280–320 nm), elicits an inflammatory response and promotes the production of ROS in the skin cells, including keratinocytes and fibroblasts. Consequently, the DNA and other cellular components in the skin cells undergo oxidative damage. The photoinduced oxidative damage activates the melanin biosynthetic pathway to protect the skin from the deleterious effects of UVR (Gray-Schopfer et al., 2007; Natarajan et al., 2014). α-Melanocyte-stimulating hormone (α-MSH), which is produced by the proteolytic cleavage of prohormone POMC, is secreted by the keratinocytes. The paracrine effect of α-MSH activates the MC1R that is located on the surface of melanocytes. The interaction between α-MSH and MC1R induces the phosphorylation of CREB through the cAMP–protein kinase A signaling pathway. The phosphorylated CREB, a transcription factor, interacts with CBP or p300 and promotes the expression of MITF, which is a key regulator of melanogenesis (Brindle et al., 1995; García-Borrón et al., 2014; Lee et al., 2012).

MITF is a member of the basic helix-loop-helix (bHLH)–leucine zipper (bHLH-LZ) transcription factor family and belongs to the MiT subfamily. The variants of MITF (MITF-A, -B, -C, -D, -E, -H, -J, -MC, -CX, and -M, among others) can be distinguished by their unique amino-terminal structure (Hartman and Czyz, 2015; Liu, 2020). These isoforms are widely expressed in various cell types, including the retinal pigment epithelium, mast cells, osteoclasts, heart cells, and melanocytes (Amae et al., 1998; Fuse et al., 1999). The melanocyte-specific MITF, MITF-M, regulates the expression of melanogenesis-related enzymes, such as tyrosinase (TYR), TYRP-1, and TYRP-2 (Goding and Arnheiter, 2019; Shibahara et al., 2000). Hence, MITF-M is a potential therapeutic target for skin hyperpigmentation disorders, such as melasma and freckles (Kumari et al., 2018).

Various MITF inhibitors have been developed to achieve skin depigmentation through different mechanisms (Pillaiyar et al., 2017). The adamantyl benzylbenzamide derivative, AP736, suppresses the MITF expression by inhibiting the cAMP–protein kinase A–CREB signaling pathway (Shin et al., 2015). The transcriptional activity of MITF is regulated by phosphorylation or sumoylation of its serine residues at positions 73 and 409. In addition, MITF transcriptional activity can be regulated by several protein inhibitors, such as activated signal transducer and activator of transcription 3

[1]*Department of Anatomy and Cell Biology, School of Medicine, Kangwon National University, Chuncheon, Republic of Korea;* [2]*Biocenter, Gyeonggido Business & Science Accelerator, Suwon, Republic of Korea;* [3]*Department of Oral Pathology, Oral Cancer Research Institute, College of Dentistry, Yonsei University, Seoul, Republic of Korea;* [4]*Department of Life Science, Ewha Womans University, Seoul, Republic of Korea;* [5]*Western Seoul Center, Korea Basic Science Institute, Seoul, Republic of Korea; and* [6]*Department of Pathology, School of Medicine, Kangwon National University, Chuncheon, Republic of Korea*

[7]*These authors contributed equally to this work.*

Correspondence: Jang-Hee Hahn, Department of Anatomy and Cell Biology, School of Medicine, Kangwon National University, Chuncheon 24341, Republic of Korea. E-mail: jhahn@kangwon.ac.kr

Abbreviations: α-MSH, α-Melanocyte-stimulating hormone; AMC, 7-amino-4-methylcoumarin; bHLH, basic helix-loop-helix–leucine; bHLH-LZ, basic helix-loop-helix–leucine zipper; ChIP, chromatin immunoprecipitation; TYR, tyrosinase

Received 15 June 2020; revised 23 December 2020; accepted 20 January 2021; accepted manuscript published online XXX; corrected proof published online XXX

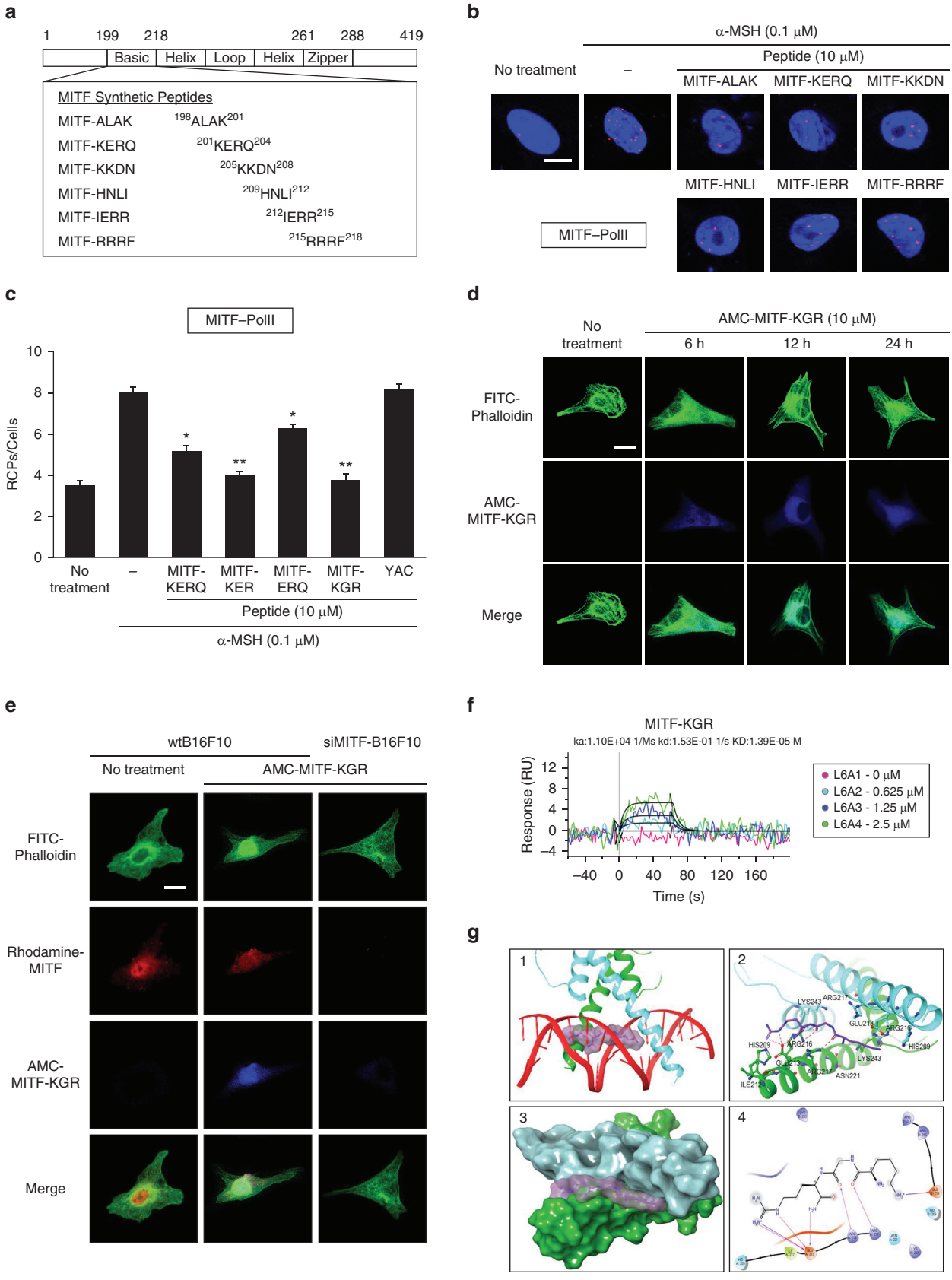

Figure 1. Identification and characterization of MITF antagonistic peptides from the conserved bHLH domain of MITF. (**a**) Schematic diagram of MITF-peptide variants. (**b**) To identify the crucial amino acid sequences, B16F1 melanoma cells were treated with 10 μM MITF-peptide (ALAK, KERQ, KKDN, HNLI, IERR, and RRRF) for 72 h in the presence of α-MSH (0.1 μM). The interaction between MITF and PolII was analyzed by in situ PLA. The red dot indicates the physical interaction between the indicated molecules. Nuclei were stained with DAPI (blue fluorescence). Magnification: ×600; Bar = 5 μm. (**c**) B16F1 melanoma cells were treated with 10 μM MITF-peptide (KERQ, KER, ERQ, KGR, and YAC) for 72 h in the presence of α-MSH (0.1 μM). PLA signals in the cell population (n = 10)

(PIAS3) and protein kinase C inhibitors. The post-translational modification of MITF, such as sumoylation, phosphorylation, or ubiquitination, can also be targeted for modulating the melanogenesis (Chen et al., 2014). Unlike modulators of signaling pathways or post-translational processes, targeted inhibitors of MITF–DNA binding can directly modulate melanocyte pigmentation. The small molecule inhibitors of MITF-E-box DNA binding were reported to decrease the melanogenic activity of MITF (Um et al., 2012). Furthermore, caffeic acid phenyl ethyl ester markedly inhibits the binding of MITF to the M-box region of the TYR, TYRP-1, and TYRP-2 promoters (Lee et al., 2013).

In this study, we investigated the inhibitory effects of MITF-KGR, a MITF basic domain–derived tripeptide, on melanogenesis and its underlying mechanism in vitro and in vivo. Our study showed that MITF-KGR exerts an antagonistic effect against α-MSH– and UVB-induced melanin synthesis by disrupting the binding of the MITF transcriptional complex to the promoter region of the target genes.

RESULTS

Cell penetrating MITF-derived peptides suppress the α-MSH–induced assembly of the transcription complex involving MITF and RNA polymerase II in B16 melanoma cells

Previous studies have shown that the conserved bHLH domain is involved in DNA binding as well as in dimerization of MITF (Hallsson et al., 2007; Raviv et al., 2014). Interestingly, most *MITF* mutations associated with Waardenburg syndrome and Tietz syndrome are located in the basic domain of the protein, which plays a major role in DNA binding (Grill et al., 2013). On the basis of these studies, we prepared a series of synthetic tetramer peptides covering the basic domain of MITF-M and examined their antagonistic activity against MITF-M–mediated transcriptional activation (Figure 1a). We hypothesized that the peptides, which inhibit the MITF–DNA binding, can also interfere with the formation of the transcription factor complex involving MITF and RNA polymerase II, which in turn plays a key role in regulating melanogenic enzyme production. In situ proximity ligation assay was performed to analyze the inhibitory effect of tetrapeptides on α-MSH–induced MITF–RNA polymerase II interaction in the murine melanoma cell line B16F1. Although most tetrapeptides inhibited the assembly of those two transcription factors, MITF-KERQ exhibited the most significant inhibitory effect (Figure 1b). Next, we compared the antagonistic efficacy of MITF-KERQ and that of its trimer derivatives to identify the smallest and most effective lead compound. MITF-KGR, in which the glutamic acid 203 was substituted with glycine, was the most effective trimer that inhibited the interaction between MITF and RNA polymerase II (Figure 1c). Contrastingly, the control tripeptide, EGF-YAC, did not affect the MITF–RNA polymerase II interaction (Yoo et al., 2014). Remarkably, 7-amino-4-methylcoumarin (AMC)–labeled MITF-KGR penetrated both the nuclear membrane and outer cell membrane of the melanocytes in a time-dependent manner, suggesting that MITF-KGR can inhibit MITF-mediated transcriptional activation in the nucleus (Figure 1d). It is worth noting that MITF and AMC-labeled MITF-KGR colocalized in the nucleus of B16F10 melanoma cells, which was not observed in the *MITF*-knockdown B16F10 melanoma cells (Figure 1e), suggesting that MITF-KGR directly binds to MITF. We performed a surface plasma resonance analysis to verify the direct interaction between MITF-KGR and MITF. The surface plasma resonance sensorgram showed efficient binding of MITF-KGR to recombinant human MITF (Figure 1f). The equilibrium dissociation constant value of MITF-KGR binding to MITF was calculated as 13.9 μM. The possible interaction of MITF-KGR with MITF was assessed by molecular docking analysis. To identify a potential binding pocket for MITF-KGR, we used the SiteMap program of the Schrödinger software (Schrödinger, New York, NY) and finally selected a binding site that includes the DNA-binding region and homodimeric protein–protein interface in MITF. In the docking model of MITF-KGR in MITF dimer, the peptide can pack tightly into the binding cavity formed by MITF region *N*-terminal to the DNA binding site through two favorable salt bridges that interact with glutamine 213 in each MITF monomer (Figure 1g). Especially, the amine and carbonyl groups of MITF-KGR form H-bonds with glutamine 213, arginine 216, and arginine 217 of MITF dimer. Taken together, these results suggest that MITF-KGR is able to penetrate the cytoplasm and block the binding of MITF to the promoter region by masking the DNA-binding domain of MITF, thereby inhibiting its function in the nucleus.

were quantified using NIS-Elements analysis. The average number of RCPs per cell ± SD is shown. $*P < 0.05$, $**P < 0.01$. (**d**) B16F10 cells were incubated with AMC-labeled MITF-KGR at 37 °C and 5% CO_2. At each time point, confocal images were taken to analyze the penetration of the MITF-KGR into the cells and are displayed in a compressed z-stack form. (**e**) B16F10 cells were incubated with AMC-labeled MITF-KGR for 24 h at 37 °C. Cells were stained with rhodamine-conjugated anti-MITF antibody. Cell images were obtained to analyze the internal distributions of AMC-labeled MITF-KGR and MITF transcriptional factors. (**d, e**) F-actin was detected by FITC-conjugated phalloidin. Images were analyzed using a confocal microscope. Magnification: ×600; Bar = 10 μm. (**f**) The direct interaction between rhMITF-M and MITF-KGR was determined by SPR analysis. (**g**) The docking pose of NH-KGR-NH2 peptide in MITF dimer:

1. The MITF dimer–DNA complex showing the predicted binding mode of NH-KGR-NH2 peptide. The MITF dimer (green and cyan) and the DNA (red) are shown in cartoon representation, and the NH-KGR-NH2 peptide is depicted in a purple surface style. Hydrogen bonds are indicated as red, and salt bridges are indicated as blue lines.
2. Detailed interactions between NH-KGR-NH2 peptide and MITF dimer are shown as a cartoon model, and the residues involved in the interaction with NH-KGR-NH2 peptide are presented in stick-ball style. H-bonds are indicated by red dashed lines. Salt bridges are indicated by pink dashed lines.
3. Close-up surface view of the predicted binding pose of NH-KGR-NH2 peptide to the bottom part of MITF dimer.
4. Schematic diagram (2D) showing the interactions of NH-KGR-NH2 peptide with MITF dimer.

Figures were drawn in Maestro (Schrödinger, New York, NY). α-MSH, α-melanocyte-stimulating hormone; 2D, two-dimensional; AMC, 7-amino-4-methylcoumarin; bHLH, basic helix-loop-helix; CO_2, carbon dioxide; h, hour; PLA, proximity ligation assay; polII, RNA polymerase II; RCP, rolling-circle product; rhMITF-M, recombinant human MITF-M; s, second; SPR, surface plasmon resonance.

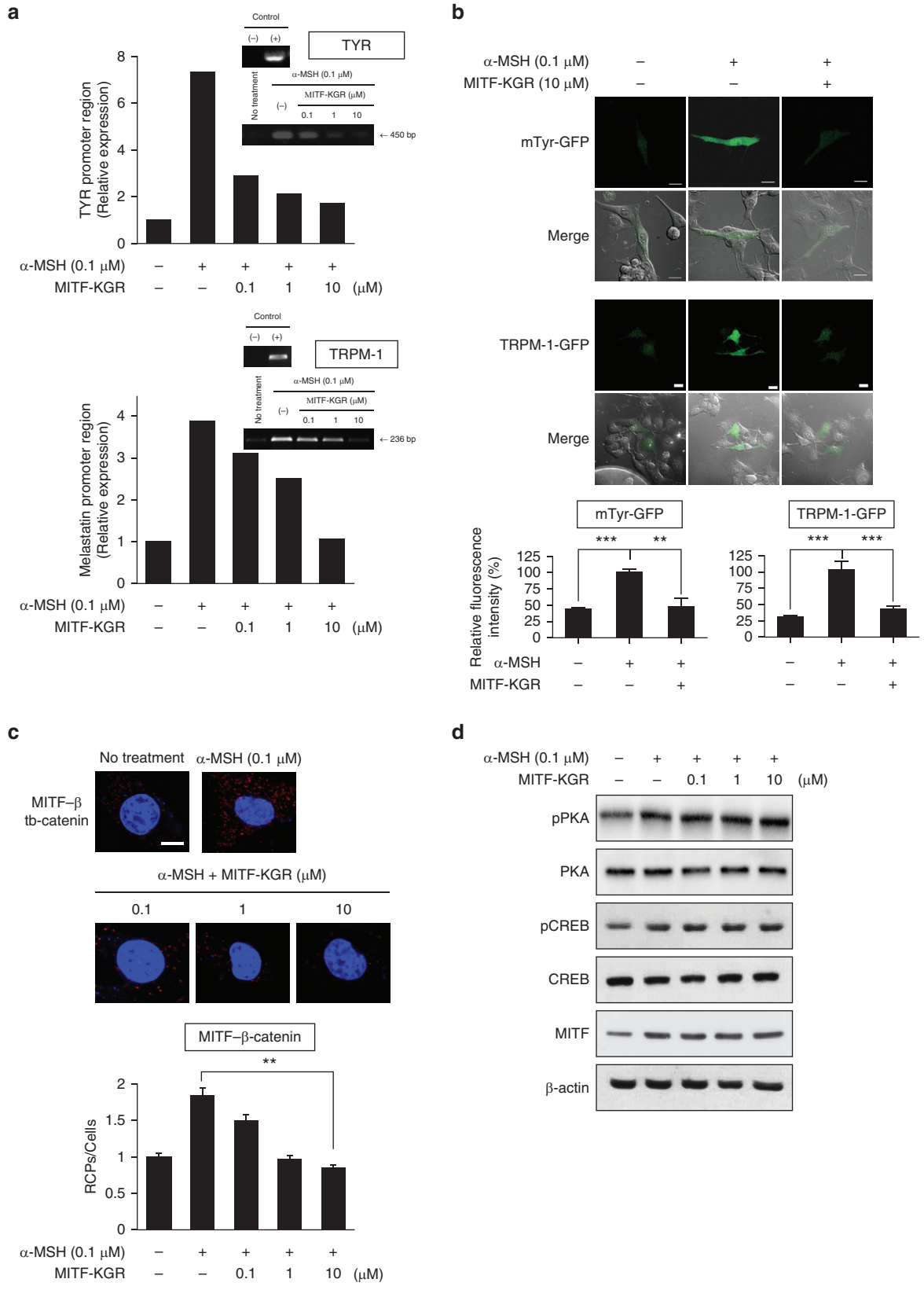

Figure 2. MITF-KGR directly inhibits the transcriptional activity of the MITF but not its expression. B16F1 melanoma cells were treated with MITF-KGR (0.1, 1, and 10 μM) in the presence of α-MSH (0.1 μM) as described earlier. (**a**) The binding of MITF to the promoter region of the gene encoding TYR or melastatin was examined by ChIP assay. (**b**) Confocal microscopy images of B16F10 melanoma cells expressing the mTyr-GFP or TRPM1–GFP (green) before and after treatment with α-MSH (100 nM) in the presence or absence of MITF-KGR (10 μM) for 24 hours. The relative fluorescence intensities (n = 6 for mTyr-GFP and n = 9 for TRPM1–GFP) were quantified using NIS Elements AR 3.0 software. $^{**}P < 0.01$, $^{***}P < 0.001$. Magnification: ×600; Bar = 20 μm. (**c**) The effect of MITF-KGR on the formation of MITF–β-catenin complex was investigated by in situ PLA. The red dot indicates the physical interaction between the indicated molecules. PLA

MITF-KGR inhibits the MITF transcriptional activity by interfering with the binding of MITF to the promoter region of downstream target genes

Chromatin immunoprecipitation (ChIP) assay was performed in the B16F1 melanoma cells to examine the inhibitory effect of MITF-KGR on the binding of MITF to the promoter region of target genes, *TYR* and melastatin (*TRPM1*). MITF-KGR exhibited a dose-dependent inhibition of α-MSH–induced enhanced binding of MITF to the promoters of non-melanogenic as well as melanogenic genes (Figure 2a). In addition, the inhibitory activity of MITF-KGR on the gene expression of *TYR* and *TRPM1* was evaluated using the mTyr-GFP plasmid containing mouse TYR promoter or TRPM1–GFP plasmid containing human melastatin promoter. MITF-KGR inhibited the α-MSH–induced expression of mTyr-GFP and TRPM1–GFP in the B16F10 melanoma cells (Figure 2b). MITF is a transcription factor that interacts with the transcriptional coactivator β-catenin and promotes the transcription of downstream target genes. We speculated that the inhibitory effect of MITF-KGR on the DNA binding of MITF may interfere with the interaction between MITF and β-catenin. In situ proximity ligation assay revealed that MITF-KGR exhibited a dose-dependent inhibition of α-MSH–induced interaction between MITF and β-catenin (Figure 2c). Next, we examined whether the MITF-KGR exerts a considerable effect on the α-MSH–induced signaling cascade and on MITF expression itself. MITF-KGR did not affect the α-MSH–induced phosphorylation levels of protein kinase A and CREB and the α-MSH–induced MITF expression as well (Figure 2d). These results suggest that MITF-KGR directly suppresses the interaction between MITF and the promoter region of the downstream target genes without affecting the α-MSH–induced signaling pathway.

MITF-KGR inhibits melanin synthesis through the downregulation of the melanogenesis-related enzymes TYR, TYRP-1, and TYRP-2

The inhibitory effect of MITF-KGR on the expression of the melanogenesis-related enzymes TYR, TYRP-1, and TYRP-2 was evaluated in two different cell lines. MITF-KGR exhibited a dose-dependent inhibition of the α-MSH–induced expression of all the three melanogenesis-related genes and proteins in the B16F1 murine melanocytes (Figure 3a and b). Similarly, MITF-KGR inhibited the expression levels of mRNA and protein of these three enzymes in the normal human melanocytes (Figure 3c and d). The melanin synthesis rate was correlated with the decreased expression of the melanogenesis-related enzymes (Figure 3e and f). Furthermore, melanin production was also significantly inhibited on treatment with different doses of MITF-KGR (Figure 3g). However, treatment with MITF-KGR did not affect dendrite formation in melanocytes. These results suggest that MITF-KGR exerts its antimelanogenic activity by downregulating the melanogenesis-related downstream target genes, not other physiological processes.

MITF-KGR attenuates the transcriptional activity of MITF in vivo

To confirm the skin-penetrating ability of MITF-KGR, we employed a reconstructed human skin model, Neoderm-M. MITF-KGR penetrated through the epidermis 3 hours after its topical application and reached the dermis layer 24 hours after the application (Figure 4a). To further investigate the antimelanogenic effect of MITF-KGR on human skin pigmentation, a melanocyte-containing reconstructed human skin model, Neoderm-ME, was used. UVB irradiation prominently increased melanin synthesis in the epidermis (Figure 4b). In contrast, MITF-KGR significantly inhibited UVB-induced melanin synthesis. These results indicate that MITF-KGR autonomously penetrates the dermis and effectively inhibits melanin biosynthesis in human skin.

To determine the role of MITF-KGR in melanogenesis in vivo, we examined the inhibitory effects of the peptide on UVB-induced skin pigmentation in melanin-possessing hairless mice (HRM2 hairless mice). Mice were treated according to the experimental plan described in Figure 5a. Mice treated with MITF-KGR for 3 days before UVB irradiation did not show any skin irritation. Repeated UVB irradiation induced pigmentation on the dorsal skin of HRM2 mice (Figure 5b). Treatment with MITF-KGR significantly reduced skin pigmentation compared with vehicle treatment. Consistent with this result, skin sections (hematoxylin stained only) indicated that the repeated UVB irradiation led to melanin accumulation in the basal layer of the epidermis (Figure 5d). In contrast, treatment with MITF-KGR significantly reduced skin pigmentation compared with vehicle treatment. MITF-KGR–treated mice showed fewer melanin spots than UVB-irradiated vehicle controls. Next, we investigated whether MITF-KGR directly affects UVB-induced expression of melanogenesis-related genes. Repeated UVB irradiation upregulated the expression of MITF and melanogenic enzymes TYR, TYRP -1, and TYRP-2 (Figure 5c). As expected, MITF-KGR suppressed the expression of TYR, TYRP-1, and TYRP-2 in a dose-dependent manner but did not affect MITF expression. Notably, the topical application of MITF-KGR also had an inhibitory effect on the UVB-induced thickening of the epidermis (Figure 5e). Previous studies showed that MITF may be involved in UV-induced epidermal thickening (Amaro-Ortiz et al., 2013; El-Abaseri et al., 2006; Hruza and Pentland, 1993; Jin et al., 2010). Consistent with these studies, treatment with MITF-KGR significantly reduced UVB-induced melanocyte proliferation and production of proinflammatory cytokine TNF-α (Figure 5f). These results suggest that MITF-KGR effectively not only suppresses the expression of melanogenic genes but also attenuates UVB-induced epidermal thickening through the suppression of MITF activity.

DISCUSSION

Previous studies on the inhibition of melanin synthesis reported that the dimeric or trimeric bioactive peptides

signals in the cell population (n = 10) were quantified using NIS-Elements analysis. The average number of RCPs per cell ± SD is shown. $^{**}P < 0.01$. Magnification: ×600; Bar = 5 μm. (**d**) Whole-cell lysates were subjected to SDS-PAGE and were analyzed using western blotting with the indicated antibodies. α-MSH, α-melanocyte-stimulating hormone; bp, base pair; ChIP, chromatin immunoprecipitation; pCREB, phosphorylated CREB; PKA, protein kinase A; PLA, proximity ligation assay; pPKA, phosphorylated protein kinase A; RCP, rolling-circle product; TYR, tyrosinase.

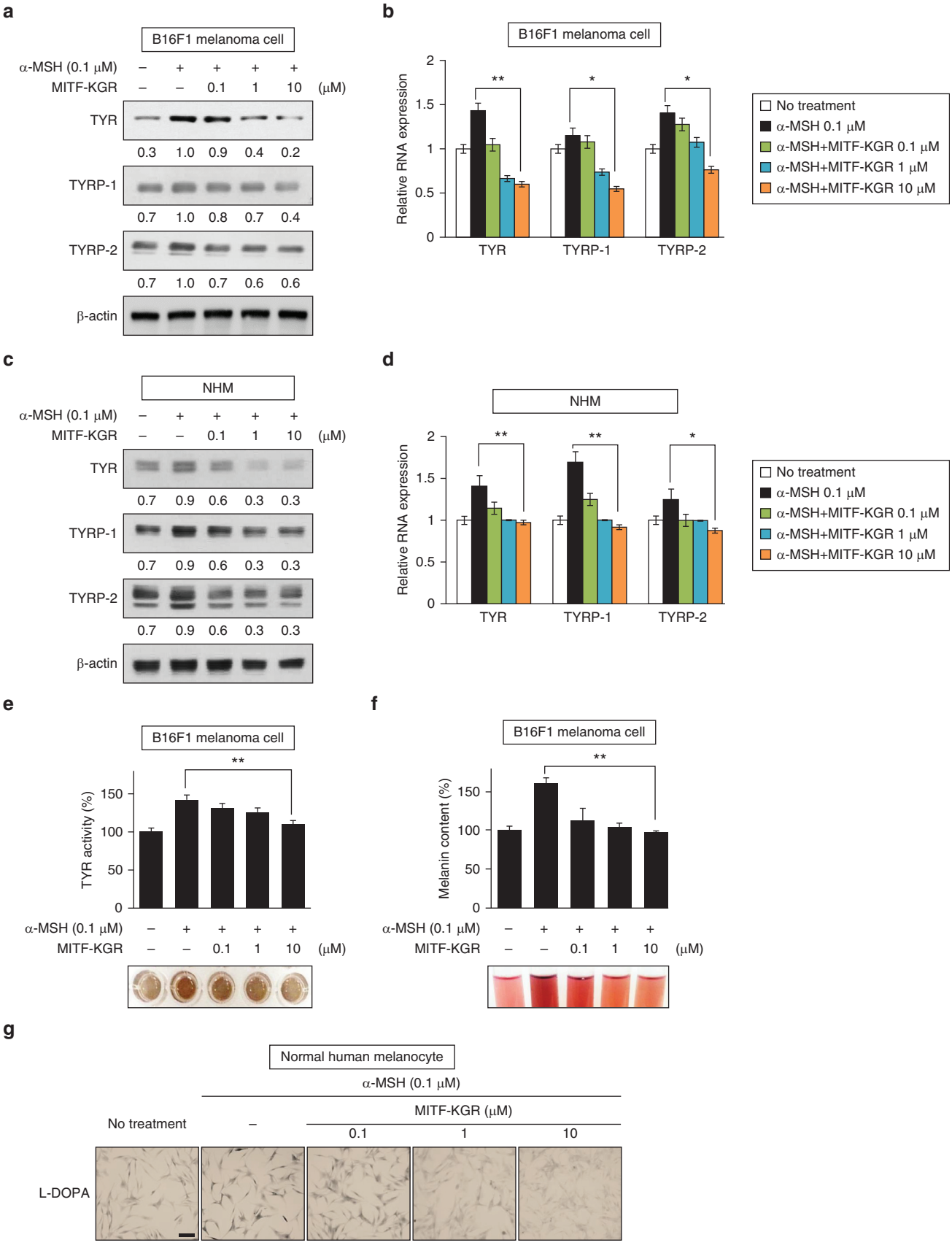

Figure 3. MITF-KGR tripeptide inhibits melanin synthesis by suppressing the expression of melanogenesis-related enzymes. B16-F1 melanoma cells or NHMs were cultured for 72 hours in DMEM supplemented with MITF-KGR (0.1, 1, or 10 μM) and α-MSH (0.1 μM). (**a, c**) Whole-cell lysates were subjected to SDS-PAGE and analyzed using western blotting with the indicated antibodies. β-Actin was used as the loading control. (**b, d**) The relative RNA expression of the enzymes related to melanin synthesis was analyzed by QRT-PCR. The lines indicate statistical comparisons, and the significant differences from the α-MSH

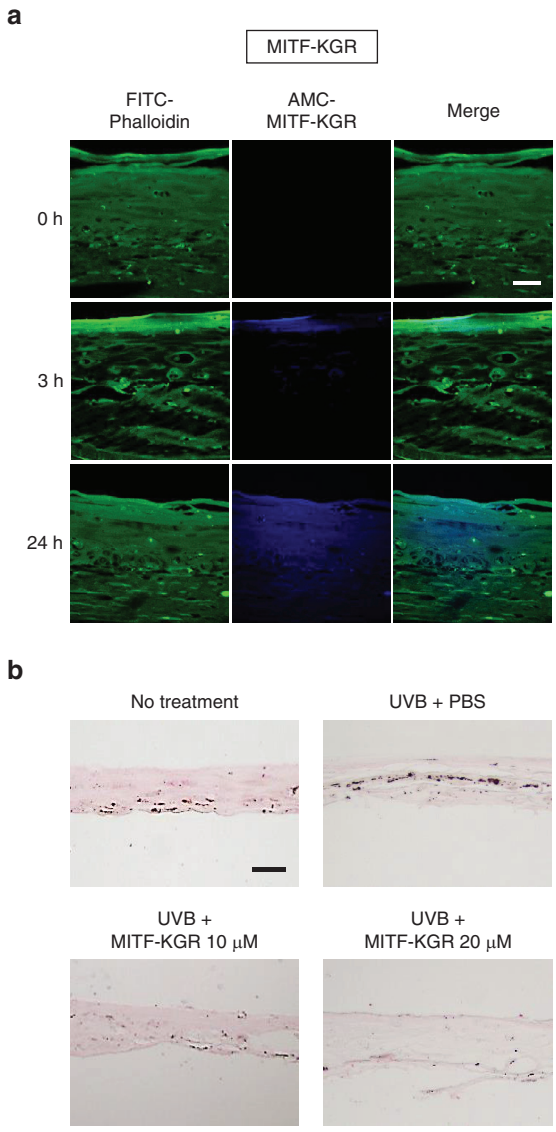

Figure 4. The inhibitory effect of MITF-KGR on melanin synthesis in reconstructed human skin models Neoderm-M and Neoderm-ME. (**a**) Neoderm-M was treated with 10 μM of AMC-labeled MITF-KGR. The reconstituted human skin was fixed with 4% PFA and permeabilized with 0.05% Triton X-100 for 10 minutes at room temperature and was then embedded in paraffin and cut into 4-μm thick sections. The sections were stained with FITC-conjugated phalloidin to identify the localization of AMC-labeled MITF-KGR. Localization of AMC-labeled MITF-KGR in the epidermal and dermal layers of the skin model was imaged at an excitation wavelength of 405 nm using a confocal microscope. Bar = 30 μm. (**b**) Neoderm-ME was treated with 10 μM or 20 μM of MITF-KGR 3 h before and just after UVB irradiation. The reconstructed human skin was irradiated with 60 mJ/cm^2 UVB every 2 days. The melanin content was visualized by Fontana-Masson staining and imaged using a bright-field microscope. Bar = 30 μm. AMC, 7-amino-4-methylcoumarin; h, hour; PFA, paraformaldehyde.

downregulate the expression of MITF, which subsequently downregulates the expression of melanogenic genes and results in skin hypopigmentation (Choi et al., 2016; Kim et al., 2012; Lee et al., 2012). In this study, we reported the tripeptide inhibitor of MITF-DNA binding that is, to our knowledge, previously unreported. MITF-KGR strongly suppressed the expression of the melanogenesis-related enzymes TYR, TYRP-1, and TYRP-2. However, treatment with MITF-KGR did not activate the upstream signaling molecules, such as protein kinase A and CREB, which were induced by treatment with α-MSH. These results indicate that the MITF-derived peptide directly regulates the transcriptional function of MITF and not its expression.

MITF-KGR is an extrinsic functional competitive inhibitor, which was derived from the conserved bHLH-LZ domain. The 12 variants of MITF among the 13 known human variants share a bHLH-LZ DNA-binding and/or dimerization domain (Hartman and Czyz, 2015). The proteins of this family share a basic DNA-binding region and an HLH–leucine zipper domain, which is important for dimerization. The bHLH is a characteristic protein structural motif of one of the largest families of dimerizing transcription factors (Amoutzias et al., 2008). The bHLH transcription factors are often important during development or cell functions. In bHLH transcription factors, there are two signals located in the DNA-binding region, spanning the residues 197–206 and 214–217, whereas the third signal is present in the bHLH-LZ domain, spanning the residues 255–265 (Fock et al., 2019). As mentioned previously, MITF-KGR was derived from the conserved bHLH-LZ domain, and it also belongs to the DNA-binding region.

Lysine 202 and arginine 204 residues are evolutionarily conserved between humans and *Drosophila melanogaster* (Holowatyj et al., 2015). Interestingly, lysine residue is the site for the interaction between MITF and p300 cofactor (Hartman and Czyz, 2015). Our data revealed that MITF-KER and MITF-KGR markedly inhibit the interaction between MITF and RNA polymerase II, whereas MITF-ERQ did not affect the interaction. Hence, lysine 202 residue plays a key role in the MITF-DNA binding. Arginine 204 is a hot spot for the human germline *MITF* mutation, which indicates its functional significance. Because lysine 202 and arginine 204 are located in the basic domain, we speculated that MITF-KGR can competitively inhibit the binding of MITF to the TYR promoter region. ChIP assay revealed that treatment with MITF-KGR resulted in dose-dependent inhibition of the α-MSH–induced binding of MITF to the promoter region of the *TYR* gene. Moreover, MITF-KGR inhibited the α-MSH–induced interaction between MITF and β-catenin complexes. MITF-KGR might modulate the binding stability of MITF to the *TYR* gene promoter, which decreases the interaction of MITF with β-catenin. Consistently, MITF-KGR exhibited a dose-dependent inhibition of the α-MSH–induced expression of all the three melanogenesis-related genes and melanin in the B16F1 murine melanocytes and the normal human melanocytes. However, MITF-KGR did not have any inhibitory effect on the UVB-induced expression of MITF. Together, these results suggest that MITF-KGR may affect the

treatment are shown by asterisks as follows: *$P < 0.05$, **$P < 0.01$. (**e**) The TYR activity and (**f**) melanin content were determined by measuring the absorbance at 490 nm. (**g**) NHMs were cotreated with MITF-KGR (0.1, 1, or 10 μM) in α-MSH (0.1 μM) for 120 hours. The TYR was determined by L-DOPA staining. Images were captured under identical conditions using a bright-field microscope. Bar = 100 μm. α-MSH, α-melanocyte-stimulating hormone; NHM, normal human melanocyte; QRT-PCR, quantitative real-time reverse transcriptase–PCR; TYR, tyrosinase.

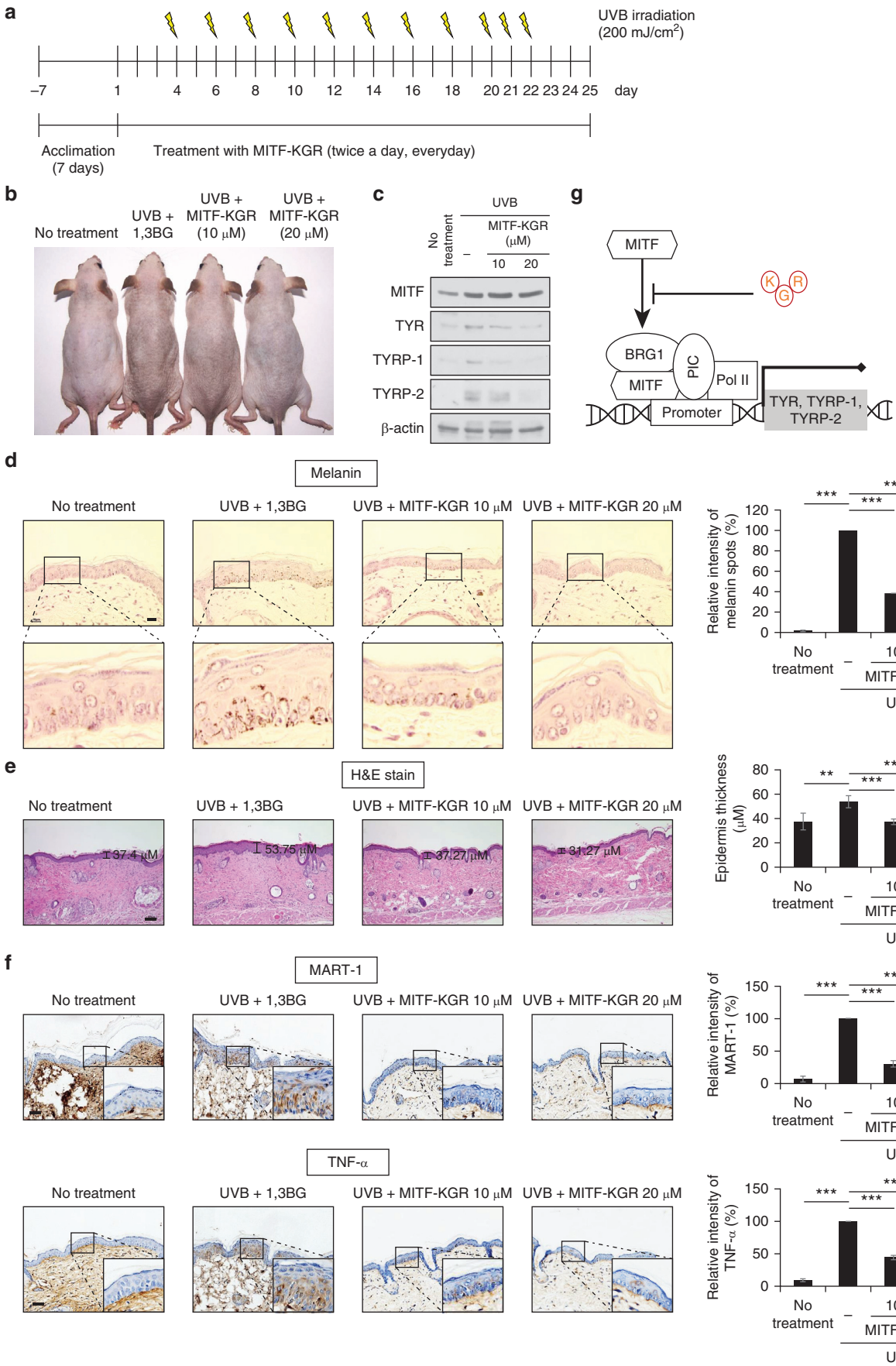

Figure 5. Histological analysis of a cross-section of the skin topically treated with MITF-KGR. (**a**) HRM2 mice were exposed to 312 nm UVB and were then treated with MITF-KGR (10 and 20 μM) or 1,3BG (vehicle control solvent) as described in Materials and Methods. The mice were irradiated 11 times at the

transcriptional activity of MITF as a transcription factor for downstream target genes.

MITF-KGR also significantly inhibited melanocyte proliferation and inflammatory cytokine release in the UVB-irradiated dorsal skin of the mice, which led to inhibition of epidermis thickening. MITF has been shown to upregulate the expression of genes involved in cell survival and proliferation (Goding and Arnheiter, 2019). Consistently, our in vivo results indicate that MITF-KGR can function as an inhibitor of pro-proliferative function for MITF. However, it remains elusive how MITF-KGR suppresses UV-induced inflammatory cytokine release. Contrary to our results, a previous study reported that MITF represses inflammatory responsiveness by decreasing c-Jun expression (Riesenberg et al., 2015). At this moment, we cannot rule out the possibility that MITF-KGR suppresses inflammation through its unknown effect, which leads to the reduction of pigmentation. In this regard, our results suggest that MITF-KGR might reduce melanogenesis by the suppression of not only MITF activity but also inflammation.

Given that dendrite formation in melanocytes is correlated with melanin production in the transportation of melanosome first to the dendritic tips and then to the keratinocytes (Scott, 2002; Scott and Cassidy, 1998), it is notable that MITF-KGR significantly inhibited melanin production, whereas it had no inhibitory effect on dendrite formation in melanocytes. This shows that MITF-KGR may only affect MITF-mediated melanin synthesis by interrupting the interaction of MITF with other transcription factors but not other cellular responses.

Collectively, we showed that the basic region-derived peptides of MITF inhibit the expression of the melanogenesis-related enzymes, namely TYR, TYRP-1, and TYRP-2, by suppressing the binding of MITF to the promoter region of the downstream target genes, subsequently blocking melanin synthesis (Figure 5g). Furthermore, these peptides blocked the UVB-mediated epidermal thickening in the mice. These results suggest that the MITF-derived peptide MITF-KGR has therapeutic potential in MITF-related skin disorders, including solar lentigo, by suppressing MITF transcriptional activity in human melanocytes.

MATERIALS AND METHODS

Cell culture and transfection

The murine melanoma cell lines, B16F1 and B16F10, were purchased from ATCC (Manassas, VA). The normal human melanocytes were purchased from Korean Cell Line Bank. Transfection with small interfering RNA, cell stimulation, and western blotting analysis are described in the Supplementary Materials and Methods.

Plasmids

The details of the plasmids used are provided in the Supplementary Materials and Methods.

Synthesis of MITF-derived peptides

The MITF-derived peptides were synthesized using an automatic peptide synthesizer (PeptrEX-R48; Peptron, Daejeon, Republic of Korea), following the manufacturer's instructions. The synthesized polypeptides were purified and characterized by reverse-phase high-performance liquid chromatography (Prominence LC-20AB; Shimadzu, Kyoto, Japan) and mass spectrometry (HP1100 Series LC/MSD; Hewlett-Packard, Palo Alto, CA).

Quantification of melanin content

The effects of UVR on melanogenesis were evaluated using the B16F1 melanoma cells, following the previously described protocol with minor modifications (Amoutzias et al., 2008). The details are described in the Supplementary Materials and Methods.

TYR activity

The TYR activity was determined following a previously described protocol with minor modifications (Bertolotto et al., 1998). The details are described in the Supplementary Materials and Methods.

In situ L-DOPA staining

The in situ enzymatic activity of TYR was measured by L-DOPA staining. The normal human melanocytes were grown on coverslips and fixed with 4% paraformaldehyde for 15 minutes and permeabilized with 0.1% Triton X-100 for 5 minutes. The cells were washed with PBS and incubated with 0.1% L-DOPA (Sigma-Aldrich, St. Louis, MO) prepared in PBS (pH 6.8) for 3 hours at 37 °C. The cells were then rinsed in PBS, and the images were captured using an Olympus fluoview FV1000 (Olympus, Tokyo, Japan) microscope.

Live-cell fluorescence imaging

The B16F10 cells were cultured in 12-well cell culture plates containing coverslips (diameter: 18 mm) coated with poly-L-lysine (Sigma-Aldrich) for fluorescence imaging. The cells were transiently transfected with mTyr–GFP or TRPM1–GFP for 24 hours. Next, the cells were incubated with α-MSH (100 nM) in the presence of MITF-KGR (10 μM) or control peptide (10 μM) for 24 hours. Live-cell imaging was performed using the Nikon A1R laser-scanning confocal microscope (Nikon, Tokyo, Japan) equipped with a heated stage chamber (LCI, Gyeonggi-do, S. Korea) and supplied with 5% carbon dioxide. Image analysis was performed with the NIS-Elements AR 3.0 software (Nikon).

Peptide penetration assay

The B16F10 cells were cultured in 24-well plates with 12 mm coverslips (Paul Marlenfeld GmbH, Lauda-Königshofen, Germany). Alternatively, the cells were transfected with small interfering RNA against *MITF* mRNA (Santa Cruz Biotechnology, Dallas, TX). The

indicated doses (200 mJ/cm^2). (**b**) The photographs indicate the differences in pigmentation between the dorsal skins of the experimental mice. As shown in the photographs, changes in skin tone are visible. (**c**) UVB-induced expression of melanogenesis-related proteins (MITF, TYR, TYRP-1, and TYRP-2) was analyzed by SDS-PAGE. β-Actin was used as a loading control. (**d**) The skin tissue sections were stained with hematoxylin only to detect UVB-increased melanin (dark brown dots) in the basal layer of the epidermis. Representative images are shown at ×40 magnification. Bar = 20 μm. The bar graph shows the mean ± SD (n = 5) of the intensity of brown dots. Statistical significance between treatment groups is denoted by asterisks: ***$P < 0.001$. (**e**) The mouse skin sections were subjected to H&E staining. Images were captured under identical conditions using a bright-field microscope. Representative images are shown at ×10 magnification. Bar = 100 μm. The bar graph shows the mean ± SD (n = 5) of the epidermal thickness. Statistical significance between treatment groups is denoted by asterisks: **$P < 0.01$, ***$P < 0.001$. (**f**) The relative expressions of MALT-1 and TNF-α were measured using SABIA software (SABIA, San Diego, CA). Representative images are shown at ×40 magnification. Bar = 20 μm. The bar graph shows the mean ± SD (n = 5) of the intensity of brown stains on the epidermis. Statistical significance between treatment groups is denoted by asterisks: ***$P < 0.001$. (**g**) MITF-KGR can exhibit an inhibitory effect on melanogenesis by suppressing the binding of MITF to the promoter regions of *TYR*, *TYRP-1*, and *TYRP-2*. 1,3BG, 1,3-butylene glycol; PIC, preinitiation complex; polII, RNA polymerase II; TYR, tyrosinase; TYRP-1, tyrosinase-related protein-1; TYRP-2, tyrosinase-related protein-2.

cells were time-dependently incubated with serum-free DMEM containing 10 μM of AMC-labeled MITF-KGR at 37 °C. After incubation, the cells were washed with PBS three times. To confirm the colocalization of MITF and AMC-labeled MITF-KGR, the cells were stained with anti-MITF antibody and rhodamine-conjugated secondary antibody. F-actin was detected using FITC-conjugated phalloidin. The cells were imaged at an excitation wavelength of 405 nm using a confocal microscope (Fluoview FV1000; Olympus).

RNA extraction and quantitative real-time reverse transcriptase–PCR

Total RNA was extracted from the cell lysates using the Total RNA Purification Kit (NanoHelix, Daejeon, Republic of Korea), and cDNA was prepared using an RT-premix (ELPIS-Biotech, Daejeon, Republic of Korea), following the manufacturer's instructions. The oligonucleotide primers were purchased from Bioneer (Daejeon, Republic of Korea). Quantitative real-time reverse transcriptase–PCR was performed using Rotor-Gene Q (Qiagen, Hilden, Germany). The details of primers are provided in the Supplementary Table S1. The PCR products were resolved on 1% agarose gel by electrophoresis and were visualized under UV light. The target gene expression was normalized against the expression of the housekeeping gene, *GAPDH*. Relative quantification of expression level was performed using the comparative $\Delta\Delta C_t$ method, following the manufacturer's instructions.

Western blotting

Western blotting was performed as described previously (Lee et al., 2017). The details are provided in the Supplementary Materials and Methods.

ChIP assay

ChIP assay was performed using the ChIP assay kit (Merck Millipore, Darmstadt, Germany), following the manufacturer's instructions. Briefly, the cells were fixed with 1% formaldehyde, and the cell pellet was sonicated in the lysis buffer. The lysate was centrifuged, and the supernatant was diluted and precleared with salmon DNA and/or protein in agarose 50% slurry (Thermo Fisher Scientific, Waltham, MA) for 30 minutes at 4 °C. The precleared supernatant was incubated overnight at 4 °C with anti-MITF antibody and isotype IgG (all from Santa Cruz Biotechnology). The target genes in the precipitated DNA and input genomic DNA were amplified by PCR using the following primers: *TYR* (−404 to +46), forward, 5′-GAGGCAACTATTTTAGACTGATTACTTT-3′ and reverse, 5′-GAAGTCTGTGACACTCATTAACCT-3′ and *TRPM1* (−429 to −194), forward, 5′-GAGCAACCAAGCCTGTAAGC-3′ and reverse, 5′-TCCAGCAAGGTGAAATGTGA-3′. The PCR products were resolved on a 2% agarose gel and visualized under UV light.

In situ proximity ligation assay

In situ proximity ligation assay was performed using a kit (Duolink In Situ reagents; O-LINK Bioscience, Uppsala, Sweden), following the manufacturer's instructions as described previously (Lee et al., 2017).

Surface plasmon resonance assay

Binding kinetics and affinities of MITF-KGR to recombinant human MITF (OriGene, Rockville, MD) were assessed using a ProteOnXPR36 (Bio-Rad Laboratories, Hercules, CA). The GLH sensor chip (Bio-Rad Laboratories) was activated with 1-ethyl-3-(3-dimethylaminopropyl) carbodiimide hydrochloride and N-hydroxysulfosuccinimide according to the manufacturer's instructions. Recombinant human MITF was successfully immobilized to a surface density of 4,000 response units by injecting 300 μl of 6 ng/μl solution (pH 4.5) at a flow rate of 30 μl/min. Kinetic data were obtained by injecting different concentrations of MITF-KGR (from 0.625 to 2.5 μM in PBS with Tween 20 containing 1 % DMSO) onto the sensor chip at a flow rate of 100 μl/min, and the association and dissociation behavior were compared. Peptide binding affinities were measured and calculated by the response units. The equilibrium dissociation constant was derived by a Langmuir model using the ProteOn Manager software (Bio-Rad Laboratories).

Molecular docking analysis

To determine the binding mode of NH-KGR-NH2 peptide to MITF, the crystal structure was retrieved from the RCSB Protein Data Bank (Protein Data Bank Identification: 4ATI). Molecular docking studies were performed using the Glide software (Schrödinger), which uses an optimized potential for liquid simulations-2005 force field, and refinement was carried out as per the recommendations of the Schrödinger Protein Preparation Wizard (Jacobson et al., 2004, 2002). LigPrep was used to generate three-dimensional structures of the ligands. The active binding sites of NH-KGR-NH2 were identified using the modeled protein structure in the SiteMap program of the Schrödinger software (Halgren, 2009). On a defined receptor grid, flexible docking was performed using the standard precision mode of Glide (Friesner et al., 2004). The best docking pose for a compound was selected on the basis of the best-scoring conformations obtained from the Glide program.

Reconstructed human skin model

The reconstructed human skin models, Neoderm-M and Neoderm-ME, were purchased from Tego Science (Seoul, Republic of Korea) and analyzed according to the manufacturer's instructions. The details are provided in the Supplementary Materials and Methods.

In vivo study

Animal experiments were carried out in accordance with the Declaration of Kangwon National University (Chuncheon, Republic of Korea) and were approved by a local ethics committee. The details are provided in the Supplementary Materials and Methods.

Statistical analysis

Statistical significance was tested using the Student's *t*-test. The difference was considered statistically significant when the *P*-value was <0.05.

Data availability statement

No datasets were generated or analyzed during this study.

ORCIDs

Dongyoung Lim: http://orcid.org/0000-0001-7629-1711
Kyoung-Jin Lee: http://orcid.org/0000-0002-5975-4486
Yuri Kim: http://orcid.org/0000-0002-4571-0861
Minseo Kim: http://orcid.org/0000-0001-9234-5011
Hyun-Mi Ju: http://orcid.org/0000-0001-6301-1194
Myoung-Ju Kim: http://orcid.org/0000-0002-6647-8870
Dong-Hwa Choi: http://orcid.org/0000-0002-2121-066X
Jiwon Choi: http://orcid.org/0000-0002-0786-6187
Suree Kim: http://orcid.org/0000-0003-1800-4969
Dongmin Kang: http://orcid.org/0000-0001-5997-625X
Kyoungyul Lee: http://orcid.org/0000-0002-6243-6868
Jang-Hee Hahn: http://orcid.org/0000-0003-1534-3789

CONFLICT OF INTEREST

The authors state no conflict of interest.

ACKNOWLEDGMENTS

This study was supported by a 2016Research Grant from Kangwon National University, Chuncheon, Republic of Korea (Number 520160231) and Korea Basic Science Institute (National Research Facilities and Equipment Center; Daejeon, Republic of Korea) grant funded by the Ministry of Education

(2019R1ABC1010020). We highly appreciate David E. Fisher (Department of Dermatology, Harvard Medical School, Boston, MA) for providing the MITF-responsive reporter plasmid pTRPM-1-wt.

AUTHOR CONTRIBUTIONS

Conceptualization: DL, KJL, JHH; Data Curation: DL, KJL, JHH; Formal Analysis: DL, KJL; Funding Acquisition: JHH; Investigation: DL, KJL, MK, YK, HMJ, MJK, DHC, JC, KL, SK; Project Administration: KJL, JHH; Supervision: DK, JHH; Validation: DL, KJL, JHH; Visualization: DL, HMJ, KL, SK; Writing − Original Draft Preparation: DL, KJL, JHH; Writing − Review and Editing: KJL, JHH

SUPPLEMENTARY MATERIAL

Supplementary material is linked to the online version of the paper at www.jidonline.org, and at https://doi.org/10.1016/j.jid.2021.01.037.

REFERENCES

Amae S, Fuse N, Yasumoto K, Sato S, Yajima I, Yamamoto H, et al. Identification of a novel isoform of microphthalmia-associated transcription factor that is enriched in retinal pigment epithelium. Biochem Biophys Res Commun 1998;247:710−5.

Amaro-Ortiz A, Vanover JC, Scott TL, D'Orazio JA. Pharmacologic induction of epidermal melanin and protection against sunburn in a humanized mouse model. J Vis Exp 2013;79:50670.

Amoutzias GD, Robertson DL, Van de Peer Y, Oliver SG. Choose your partners: dimerization in eukaryotic transcription factors. Trends Biochem Sci 2008;33:220−9.

Bertolotto C, Abbe P, Hemesath TJ, Bille K, Fisher DE, Ortonne JP, et al. Microphthalmia gene product as a signal transducer in cAMP-induced differentiation of melanocytes. J Cell Biol 1998;142:827−35.

Brindle P, Nakajima T, Montminy M. Multiple protein kinase A-regulated events are required for transcriptional induction by cAMP. Proc Natl Acad Sci USA 1995;92:10521−5.

Chen H, Weng QY, Fisher DE. UV signaling pathways within the skin. J Invest Dermatol 2014;134:2080−5.

Choi HR, Kang YA, Lee HS, Park KC. Disulfanyl peptide decreases melanin synthesis via receptor-mediated ERK activation and the subsequent downregulation of MITF and tyrosinase. Int J Cosmet Sci 2016;38:279−85.

D'Mello SA, Finlay GJ, Baguley BC, Askarian-Amiri ME. Signaling pathways in melanogenesis. Int J Mol Sci 2016;17:1144.

El-Abaseri TB, Putta S, Hansen LA. Ultraviolet irradiation induces keratinocyte proliferation and epidermal hyperplasia through the activation of the epidermal growth factor receptor. Carcinogenesis 2006;27:225−31.

Fock V, Gudmundsson SR, Gunnlaugsson HO, Stefansson JA, Ionasz V, Schepsky A, et al. Subcellular localization and stability of MITF are modulated by the bHLH-Zip domain. Pigment Cell Melanoma Res 2019;32:41−54.

Friesner RA, Banks JL, Murphy RB, Halgren TA, Klicic JJ, Mainz DT, et al. Glide: a new approach for rapid, accurate docking and scoring. 1. Method and assessment of docking accuracy. J Med Chem 2004;47:1739−49.

Fuse N, Yasumoto K i, Takeda K, Amae S, Yoshizawa M, Udono T, et al. Molecular cloning of cDNA encoding a novel microphthalmia-associated transcription factor isoform with a distinct amino-terminus. J Biochem 1999;126:1043−51.

García-Borrón JC, Abdel-Malek Z, Jiménez-Cervantes C. MC1R, the cAMP pathway, and the response to solar UV: extending the horizon beyond pigmentation. Pigment Cell Melanoma Res 2014;27:699−720.

Goding CR, Arnheiter H. MITF-the first 25 years. Genes Dev 2019;33:983−1007.

Gray-Schopfer V, Wellbrock C, Marais R. Melanoma biology and new targeted therapy. Nature 2007;445:851−7.

Grill C, Bergsteinsdóttir K, Ogmundsdóttir MH, Pogenberg V, Schepsky A, Wilmanns M, et al. MITF mutations associated with pigment deficiency syndromes and melanoma have different effects on protein function. Hum Mol Genet 2013;22:4357−67.

Halgren TA. Identifying and characterizing binding sites and assessing druggability. J Chem Inf Model 2009;49:377−89.

Hallsson JH, Haflidadóttir BS, Schepsky A, Arnheiter H, Steingrímsson E. Evolutionary sequence comparison of the Mitf gene reveals novel conserved domains. Pigment Cell Res 2007;20:185−200.

Hartman ML, Czyz M. MITF in melanoma: mechanisms behind its expression and activity. Cell Mol Life Sci 2015;72:1249−60.

Holowatyj A, Yang ZQ, Pile LA. Histone lysine demethylases in Drosophila melanogaster. Fly (Austin) 2015;9:36−44.

Hruza LL, Pentland AP. Mechanisms of UV-induced inflammation. J Invest Dermatol 1993;100:35S−41S.

Jacobson MP, Friesner RA, Xiang Z, Honig B. On the role of the crystal environment in determining protein side-chain conformations. J Mol Biol 2002;320:597−608.

Jacobson MP, Pincus DL, Rapp CS, Day TJ, Honig B, Shaw DE, et al. A hierarchical approach to all-atom protein loop prediction. Proteins 2004;55:351−67.

Jin XJ, Kim EJ, Oh IK, Kim YK, Park CH, Chung JH. Prevention of UV-induced skin damages by 11,14,17-eicosatrienoic acid in hairless mice in vivo. J Korean Med Sci 2010;25:930−7.

Kim SY, Na JI, Park SJ, Choi HR, Kim DS, Park KC. Novel tri-peptides with hypopigmenting activity. J Dermatol Sci 2012;65:68−9.

Kumari S, Tien Guan Thng S, Kumar Verma N, Gautam HK. Melanogenesis inhibitors. Acta Derm Venereol 2018;98:924−31.

Lee HE, Kim EH, Choi HR, Sohn UD, Yun HY, Baek KJ, et al. Dipeptides inhibit melanin synthesis in Mel-Ab cells through down-regulation of tyrosinase. Korean J Physiol Pharmacol 2012;16:287−91.

Lee JY, Choi HJ, Chung TW, Kim CH, Jeong HS, Ha KT. Caffeic acid phenethyl ester inhibits alpha-melanocyte stimulating hormone-induced melanin synthesis through suppressing transactivation activity of microphthalmia-associated transcription factor. J Nat Prod 2013;76:1399−405.

Lee KJ, Kim Y, Yoo YH, Kim MS, Lee SH, Kim CG, et al. CD99-derived agonist ligands inhibit fibronectin-induced activation of β1 integrin through the protein kinase A/SHP2/extracellular signal-regulated kinase/PTPN12/focal adhesion kinase signaling pathway. Mol Cell Biol 2017;37. e00675−16.

Liu D. Handbook of tumor syndromes. Boca Raton, FL: CRC Press; 2020.

Maresca V, Flori E, Picardo M. Skin phototype: a new perspective. Pigment Cell Melanoma Res 2015;28:378−89.

Natarajan VT, Ganju P, Ramkumar A, Grover R, Gokhale RS. Multifaceted pathways protect human skin from UV radiation. Nat Chem Biol 2014;10:542−51.

Pillaiyar T, Manickam M, Jung SH. Downregulation of melanogenesis: drug discovery and therapeutic options. Drug Discov Today 2017;22:282−98.

Raviv S, Bharti K, Rencus-Lazar S, Cohen-Tayar Y, Schyr R, Evantal N, et al. PAX6 regulates melanogenesis in the retinal pigmented epithelium through feed-forward regulatory interactions with MITF. PLoS Genet 2014;10:e1004360.

Riesenberg S, Groetchen A, Siddaway R, Bald T, Reinhardt J, Smorra D, et al. MITF and c-Jun antagonism interconnects melanoma dedifferentiation with pro-inflammatory cytokine responsiveness and myeloid cell recruitment. Nat Commun 2015;6:8755.

Scott G. Rac and rho: the story behind melanocyte dendrite formation. Pigment Cell Res 2002;15:322−30.

Scott GA, Cassidy L. Rac1 mediates dendrite formation in response to melanocyte stimulating hormone and ultraviolet light in a murine melanoma model. J Invest Dermatol 1998;111:243−50.

Shibahara S, Yasumoto K, Amae S, Udono T, Watanabe K, Saito H, et al. Regulation of pigment cell-specific gene expression by MITF. Pigment Cell Res 2000;13(Suppl. 8):98−102.

Shin HJ, Oh CT, Kwon TR, Beak HS, Joo YH, Kim JH, et al. A novel adamantyl benzylbenzamide derivative, AP736, inhibits melanogenesis in B16F10 mouse melanoma cells via glycogen synthase kinase 3beta phosphorylation. Int J Mol Med 2015;36:1353−60.

Um JM, Kim HJ, Lee Y, Choi CH, Hoang Nguyen D, Lee HB, et al. A small molecule inhibitor of Mitf-E-box DNA binding and its depigmenting effect in melan-a cells. J Eur Acad Dermatol Venereol 2012;26:1291−7.

Yoo YH, Kim YR, Kim MS, Lee KJ, Park KH, Hahn JH. YAC tripeptide of epidermal growth factor promotes the proliferation of HaCaT keratinocytes through activation of EGFR. BMB Rep 2014;47:581−6.